The International Journal of Advanced Manufacturing Technology (2018) 98:755–769
https://doi.org/10.1007/s00170-018-2304-3

ORIGINAL ARTICLE

Robust evaluation of chatter stability for milling process with uncertainties based on optimal configuration of machining position and spindle speed

Congying Deng[1] · Jianguo Miao[2] · Yi Feng[1] · Bo Wei[1]

Received: 5 February 2018 / Accepted: 5 June 2018 / Published online: 15 June 2018

Abstract
Chatter vibration in milling process is a major obstacle that limits the machining quality and productivity, which may be avoided by using stability lobe diagrams (SLDs). Many traditional models developed to predict chatter stability assume that dynamic parameters of the machine tool remain constant under operational conditions. However, these parameters such as natural frequencies, damping ratios, stiffness, and cutting force coefficients vary depending upon different aspects including spindle speed, tool wear, and machining position, reducing the accuracy of chatter prediction. In this study, a robust chatter prediction method based on conventional analytical milling stability models is presented by employing the Edge theorem and Zero Exclusion condition. In this method, optimal combinations of spindle speeds and machining positions are firstly researched to obtain higher critical depths of cut, based on the conventional stability model, modal fitting technique, Kriging model, and improved particle swarm optimization. At each combination, related nominal modal parameters and cutting force coefficients are identified, and their left and right worst-case deviations are also determined. Critical stable condition for each combination is detected by a graphic approach within the minimum and maximum bounds of uncertainties. Accordingly, a robust stability lobe diagram is obtained with related spindle speeds and critical cutting depths. The proposed method was verified by chatter tests on a real vertical machining center, demonstrating its reliability in chatter prediction compared to the conventional stability lobe diagram.

Keywords Chatter · Machining · Uncertainty · Robust stability · Edge theorem

1 Introduction

Chatter is a self-induced vibration phenomenon that can be ascribed to the variation of chip thickness under operational conditions. Its occurrence leads to poor surface finish, low productivity, increased tool wear, machine tool failure, and serious noise, which is the main obstacle to improving the part quality and maximize material removal rate (MRR) [1–3]. In view of the significance to avoid chatter, the mechanisms of dynamic machining process have been examined in detail for decades [4–6]. The developed stability lobe diagram (SLD) technique stating the relationship between the spindle speed and depth of cut is usually applied to predefining the appropriate chatter-free combinations of machining parameters [7–9].

Since Taylor first made the description of chatter vibrations in 1907, several other authors have contributed a lot of researches on this topic [10–12]. Tobias and Fishwick [7] established a chatter model and first utilized the SLD to predict the chatter stability, which was consistent with the definition that region below the lobe was stable and the above one was unstable. Subsequently, many other researchers conducted in-depth investigations of the different processing forms. Altintas and Budak [8, 12, 13] had developed a two degree of freedom (2DOF) analytical chatter model specifically for milling operations, where they introduced the Fourier approximation method and obtained the chatter-free machining parameters in the frequency domain. As this approach was proved to

✉ Bo Wei
dermiaoo@163.com

[1] School of Advanced Manufacturing Engineering, Chongqing University of Posts and Telecommunications, Chongqing 400065, People's Republic of China

[2] Chongqing Midea Universal Refrigeration Equipment Co., Ltd, 15 Rose Road, Nan'an District, Chongqing 401336, People's Republic of China

be efficient in determining the SLD, it lays a foundation to predict chatter stability. Later, the semi-discretization method, full-discretization method, and time-domain method were also developed to evaluate machining stabilities. The groundbreaking work contributed by the researchers benefit operators in appropriately selecting machining parameters.

However, in a real machining application, the deviations between the measurements and predictions are still observed. This problem can be mainly attributed to the assumption that system dynamics (machine, tool, and workpiece) and machining conditions are constant and time invariant when adopting the numerical methods to calculate stability diagrams. Nevertheless, under operational condition, there are many factors that cause the variations of system dynamics and machining conditions, leading to inaccurate predictions. For instance, wearing of the cutting edge can change the tool geometry, and then affect the cutting force coefficients [14, 15].

Uncertainty in chatter stability prediction has already been addressed in recent researches. Duncan et al. and Zhang et al. [16, 17] described several different sources that can cause tool tip responses and cutting force coefficients varied, including the measurement errors, tool wear, and nonlinear behavior. To further investigate how these uncertainties affect the chatter stability, the probabilistic theory is applied (e.g., Monte Carlo simulations) [16]. But it can be time-consuming and unavailable to identify the detailed statistic distributions of uncertain parameters since extensive experiments and simulations are needed to be conducted. Consequently, two types of approaches are generally used to estimate the robust chatter stability. One approach is based on the fuzzy arithmetic. Sims et al. [18] employed fuzzy arithmetic techniques to choose robust machining parameters and justified the deviations between theoretical and experimental behaviors. Haman et al. [19] applied fuzzy arithmetic to calculate two-dimensional stability limits, and developed fuzzy sensitivity analysis to quantify the effect of given uncertain parameters. Another type is based on the Edge theorem that examines whether the edges of a family of polynomials are stable. Park and Graham [20–22] considered uncertainties in natural frequencies and cutting coefficients, and combined Edge theorem and Zero Exclusion principle to develop a robust model that predicted the most conservative set of stability lobes.

In general, uncertain parameters are focused on modal parameters and cutting force coefficients [23]. When applying the aforementioned approaches, the uncertain parameters' nominal values and related bounds should be predetermined. Therefore, the factors that can cause uncertainties are identified to obtain more accurate nominal and extreme values. However, the works on robust chatter prediction considering the influences of machining position variations were addressed little. Ignoring the position-dependent milling behavior will narrow down the left and right worst-case deviations. Conversely, taking whole machine tool work volume into account will extend the bounds and provide a more conservative SLD, limiting the machining efficiency. Though researches have already investigate the effects caused by the position variations on modal parameters of tool tip frequency response functions (FRFs) and thus on milling stability [24, 25], applications of which in uncertain predictions are relatively few.

This paper presents a new method to facilitate robust prediction of milling stability in entire machine tool work volume, avoiding complicated theoretical calculations and providing relatively higher critical cutting depths. First, a Kriging model is established to predict the modal parameters dependent on machining position and spindle speed. Then, the related tool tip FRFs are reorganized using modal fitting technique. Furthermore, position with higher critical axial cutting depths at each given speed is obtained by combining the milling stability theory and the improved particle swarm optimization (IPSO) algorithm. At these optimal positions, a robust model considering uncertainties in related modal parameters and cutting force coefficients is developed by extending the conventional chatter stability theory, based on the Edge theorem and Zero Exclusion condition. Accordingly, a conservative SLD guaranteeing higher reliability can be obtained.

Henceforth, the remainder of this paper is organized as follows: the analytical derivation of using the Kriging model and the IPSO algorithm to determine a better machining position is presented in Section 2. A description of the Edge theorem and Zero Exclusion condition is presented in Section 3. And a theoretical approach of plotting the robust stability lobe under optimal configurations of machining positions and spindle speeds is also provided. This is followed by the case study and results discussion to verify the approach through experimental procedure in Section 4. Finally, conclusions from the current research are summarized in Section 5.

2 Methodology for obtaining optimal configuration of machining position and spindle speed

Since the varying machining position and spindle speed can cause effects on tool tip modal parameters and thus on milling stability, the configuration of machining position and spindle speed with higher critical axial cutting depths is obtained firstly based on two substeps. One is establishing the Kriging model to predict modal parameters dependent on spindle speed and machining position in x and y directions, and using the modal fitting technology to reorganize the related tool tip FRFs. The other is combing the analytical milling stability theory and the improved particle swarm optimization algorithm to find the optimal machining position at each given spindle speed in whole machine tool work volume. Then,

the further analytical robust prediction is based on the obtained optimal conditions.

2.1 2DOF milling stability theory

In general, a 2DOF system shown in Fig. 1 is usually used in analytical chatter stability prediction. The tool is considered to have two orthogonal degrees of freedom in x and y directions. Related stiffness and damping coefficients are labeled as k_x, k_y, c_x, and c_y. The general equations of motion for the 2DOF milling system can be expressed as follows:

$$\begin{Bmatrix} \Delta F_x(t) \\ \Delta F_y(t) \end{Bmatrix} = \frac{a_p K_{tc} N}{2\pi} \begin{bmatrix} a_{xx} & a_{xy} \\ a_{xy} & a_{yy} \end{bmatrix} \begin{Bmatrix} \Delta x \\ \Delta y \end{Bmatrix} = \frac{a_p K_{tc} N}{2\pi} [A] \begin{Bmatrix} \Delta x \\ \Delta y \end{Bmatrix} \tag{1}$$

where a_p is the axial cutting depth, K_{tc} is the tangential cutting force coefficient, and $[A]$ represents average directional factors:

$$\begin{aligned} a_{xx} &= \frac{1}{2}\left[-\cos\left(2\varphi_{jl}\right) + 2K_{rt}\varphi_{jl} - K_{rt}\sin\left(2\varphi_{jl}\right)\right]_{\varphi_{st}}^{\varphi_{ex}} \\ a_{xy} &= \frac{1}{2}\left[2\varphi_{jl} + \sin\left(2\varphi_{jl}\right) - K_{rt}\cos\left(2\varphi_{jl}\right)\right]_{\varphi_{st}}^{\varphi_{ex}} \\ a_{yx} &= \frac{1}{2}\left[-2\varphi_{jl} + \sin\left(2\varphi_{jl}\right) - K_{rt}\cos\left(2\varphi_{jl}\right)\right]_{\varphi_{st}}^{\varphi_{ex}} \\ a_{yy} &= \frac{1}{2}\left[\cos\left(2\varphi_{jl}\right) + 2K_{rt}\varphi_{jl} + K_{rt}\sin\left(2\varphi_{jl}\right)\right]_{\varphi_{st}}^{\varphi_{ex}} \end{aligned} \tag{2}$$

where K_{rt} is the ratio of the radial to tangential cutting force coefficient and φ_{st} and φ_{ex} are the start and exit angles of the cutting tooth. Equation (1) can be transformed into the frequency domain:

$$\{F\}e^{i\omega t} = \frac{a_p K_{tc} N}{2\pi} [A]\left(1 - e^{-i\omega_c \tau}\right)[G(i\omega_c)]\{F\}e^{i\omega_c t} \tag{3}$$

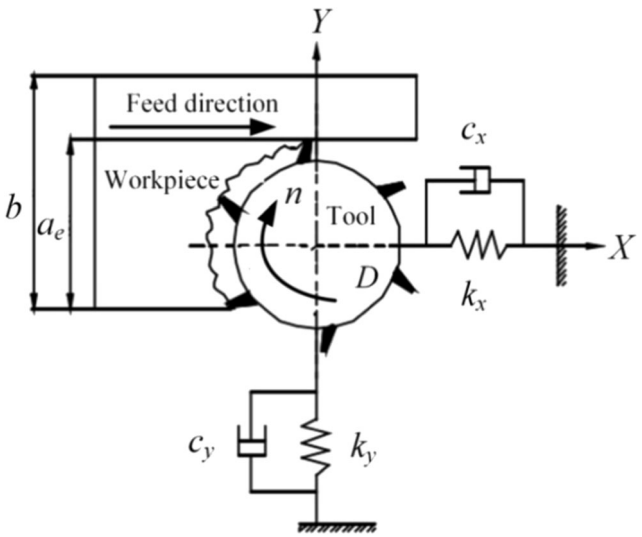

Fig. 1 2DOF milling system

$G(i\omega_c)$ is the transfer function matrix in x and y directions, which is usually represented by the tool tip FRFs since the workpiece system is more rigid than the tool system. Characteristic equation of Eq. (3) is as follows:

$$\det|I + \Lambda[G_1(i\omega_c)]| = 0 \tag{4}$$

where

$$\begin{aligned} \Lambda &= -\frac{a_p K_{tc} N}{4\pi}\left(1 - e^{-i\omega_c \tau}\right) = \Lambda_I + \Lambda_R \\ [G_1(i\omega_c)] &= \begin{bmatrix} a_{xx} & a_{xy} \\ a_{xy} & a_{yy} \end{bmatrix} \begin{bmatrix} G_{xx}(i\omega_c) & G_{xy}(i\omega_c) \\ G_{yx}(i\omega_c) & G_{yy}(i\omega_c) \end{bmatrix} \end{aligned} \tag{5}$$

where $G_{xx}(i\omega_c)$, $G_{xy}(i\omega_c)$, $G_{yx}(i\omega_c)$, and $G_{yy}(i\omega_c)$ are the direct and cross tool tip FRFs corresponding to x and y directions and Λ is the eigenvalue, which can be directly calculated from Eq. (4). Then, the axial critical cutting depth $a_{p\lim}$ can be determined with Eq. (5):

$$a_{p\lim} = -\frac{2\pi\Lambda_R\left[1 + (\Lambda_I/\Lambda_R)^2\right]}{K_{tc} N} \tag{6}$$

Equations (1) to (6) show that the milling stability is mainly dependent on the tool tip FRFs and cutting force coefficients. Thus, variations of these parameters will lead to uncertain predictions of milling stability.

2.2 Position and spindle-dependent tool tip FRF

According to the modal theory, direct transfer functions can be described by modal parameters:

$$G(s) = \sum_{r=1}^{N} \frac{\omega_{nr}/k_{er}}{s^2 + 2\xi_r\omega_{nr}s + {\omega_{nr}}^2} \tag{7}$$

where ω_{nr}, k_{er}, ξ_r, and s are the natural frequency, damping ratio, modal stiffness, and the Laplace variable respectively. If modal parameters of each mode are obtained, they can be used to reorganize $G(s)$ utilizing modal fitting technique. Since Kriging method considers the spatial correlation and variability of variables [26–28], it is adopted to establish the mathematic model to describe the relationship among modal parameters, spindle speed, and machining position. A Kriging approximate model is generally expressed as follows:

$$\hat{y}(t) = \sum_{l=1}^{p} \beta_l f_l(t) + z(t) = f^{\mathrm{T}}(t)\beta + z(t) \tag{8}$$

where $f^{\mathrm{T}}(t)$ is a regression model which is a linear combination of p chosen functions, β_l is the regression coefficient, and $z(t)$

is a random function with normal distribution $N(0, \sigma^2)$ and its covariance matrix is the following:

$$\mathrm{cov}\left(z(t_l),\ z(t_j)\right) = \sigma^2 R(t_l,\ t_j) \tag{9}$$

where $R(t_l, t_j)$ is usually represented by the Gauss function and exponential function:

$$\begin{aligned} R(t_l,\ t_j) &= \prod \exp\left(\theta_k \left| t_{lk} - t_{jk} \right|^2\right) \\ R(t_l,\ t_j) &= \prod \exp\left(\theta_k \left| t_{lk} - t_{jk} \right|\right) \end{aligned} \tag{10}$$

where θ_k is the undetermined parameter and t_{lk} and t_{jk} are the k^{th} components of t_l and t_j. Then, a correlation matrix can be formed:

$$R = \begin{bmatrix} R(t_1, t_2) & \cdots & R(t_1, t_{ns}) \\ \vdots & \cdots & \vdots \\ R(t_{ns}, t_1) & \cdots & R(t_{ns}, t_{ns}) \end{bmatrix} \tag{11}$$

A detailed derivation of Kriging predictor is presented in [25], and Eq. (8) can be transformed as Eq. (12):

$$\begin{aligned} \hat{y}(t) &= f^{\mathrm{T}}(t)\beta^* + r^{\mathrm{T}}(t) R^{-1}\left(Y^{\mathrm{T}} - F_s \beta^*\right) \\ &= f^{\mathrm{T}}(t)\beta^* + r^{\mathrm{T}}(t)\gamma^* \end{aligned} \tag{12}$$

where Y is the response matrix corresponding to the sample points, and β^* is:

$$\beta^* = \left(F_s{}^{\mathrm{T}} R^{-1} F_s\right)^{-1} F_s{}^{\mathrm{T}} R^{-1} Y \tag{13}$$

where F_s is the expended matrix on the basis of designed sites T:

$$F_s = \left[f(t_1), f(t_2), \cdots f(t_{ns})\right]^{\mathrm{T}} \tag{14}$$

According to Eq. (12), the sample matrix Y and T should be determined in advance. For establishing the Kriging model to predict modal parameters, the matrix Y contains sample modal parameters including natural frequencies, damping ratios, and modal stiffness, and the matrix T contains the spatial coordinates and spindle speeds. These sample modal parameters are identified from the related tool tip FRFs using the modal fitting technique [29].

However, during the operational state, the sample tool tip FRFs cannot be obtained directly through impact testing. Thus, finite element (FE) technology is used to establish a whole machine tool FE model considering the joint dynamics and spindle speed effects in the virtual environment. At a certain speed, different displacement combinations of the moving components are arranged to simulate different machining positions to achieve the tool tip FRFs. Then, with the sample information, the Kriging model can be established according to Eq. (12):

$$\begin{bmatrix} \omega_r(x, y, z, n) \\ \xi_r(x, y, z, n) \\ K_{er}(x, y, z, n) \end{bmatrix}^{\mathrm{T}} = f^{\mathrm{T}}(x, y, z, n)\beta^* + r^{\mathrm{T}}(x, y, z, n)\gamma^* \tag{15}$$

2.3 Optimal machining position identification

Since the improved particle swarm optimization algorithm has faster convergence speed and higher accuracy, it is adopted to find the optimal machining position. This algorithm is combined with the Kriging model and milling stability theory to perform the optimization shown in Fig. 2. The improved particle swarm optimization algorithm is a population-based optimization technique, which is initialized as a set of random solutions and searches for the optimal value iteratively [30]. In D-dimensional space, N particles are assumed to form a community. Characteristics of each particle are represented by the position $X_i = (x_{i1},\ x_{i2},\ldots,\ x_{iD})$, velocity $V_i = (v_{i1},\ v_{i2},\ldots,\ v_{iD})$ and fitness value f_i. Positions of these particles represent potential solutions to the optimization. Fitness value of each solution is evaluated based on the objective function to determine the optimal position. After one iteration, the particle best and the global best labeled as P_{best} and G_{best} are updated respectively. The two optimums are used to determine the velocities and then modify the positions of particles in the next iteration as follows:

$$\begin{cases} v_{id}^{k+1} = w v_{id}^{k} + c_1 r_1 \left(P_{best}{}_{id}^{k} - x_{id}^{k}\right) + c_2 r_2 \left(G_{best}{}_{id}^{k} - x_{id}^{k}\right) \\ x_{id}^{k+1} = x_{id}^{k} + v_{id}^{k+1} \end{cases} \tag{16}$$

where w is the inertia weight, k is the iterative number, c is the velocity weighting factors equaling 0 or positive constant, and r is the random numbers between 0 and 1.

A larger w will accelerate the convergence rate and benefit the global search, but the solution can be less accurate. A smaller w will slow the convergence rate, which can benefit the local search and obtain more accurate solution. Thus, in the iteration, w is dynamically modified based on the particles' properties. According to an IPSO algorithm, f_{avg} is the average fitness value of all particles, $f_{\max}$ is the maximum fitness value in the current iteration, and f_{havg} is the average fitness value of the particles with fitness values greater than f_{avg}. Then, the modification can be performed as follows [31]:

(i) If $f_i \le f_{avg}$, a larger w is selected considering the improvement of global research ability:

$$w = 1.2 - \frac{1 - \exp\left(-f_{\max} + f_{havg}\right)}{1 + \exp\left(-f_{\max} + f_{havg}\right)} \tag{17}$$

(ii) $f_{avg} \le f_i \le f_{havg}$ indicates these particles have better individual and global research abilities simultaneously. Thus, a larger w is determined in the initial phase, and

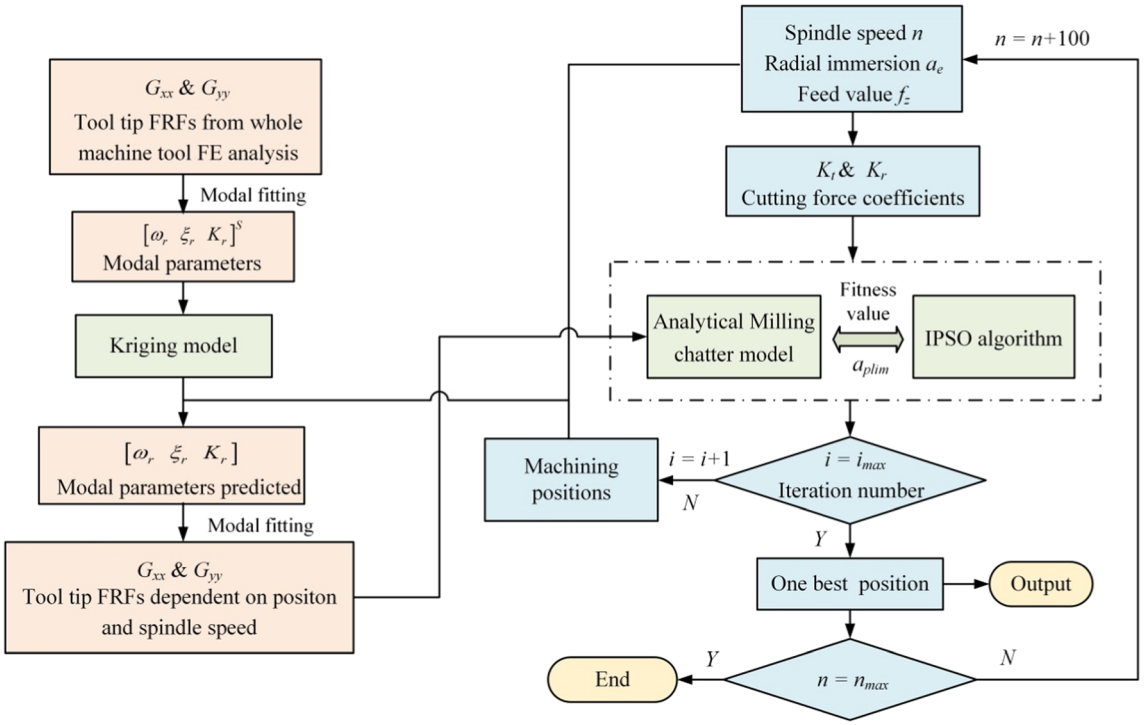

Fig. 2 Flow chart for obtaining optimal combination of spindle speeds and machining position

it is decreased gradually to improve the local research ability:

$$w = \begin{cases} w-(w-w_{\min})\left(1-\exp\left(-\dfrac{t}{t_{\max}}\right)\right) & 0\le t\le t_{\max} \\ w_{\min} & t = t_{\max} \end{cases} \quad (18)$$

(iii) if $f_{havg} < f_i \le f_{\max}$, w can be decreased appropriately to improve the local research ability:

$$w = w-w_{\min}\frac{f_i - f_{havg}}{f_{\max} - f_{havg}} \quad (19)$$

In Eqs. (17) to (19), w on the right side is still linear decreasing:

$$w = w_{\max} - \frac{w_{\max}-w_{\min}}{k_{\max}} \times k \quad (20)$$

where $k_{\max}$ is the determined maximum iterations. Furthermore, to avoid the premature convergence of the particle swarm optimization algorithm, a mutation operator is adopted to reinitialize properties of the particles with a certain probability P_m [32]:

$$P_m = 0.5 - \frac{1}{1+\exp\left[-k\left(f_{\max} - f_{havg}\right]\right.} \quad k > 0 \quad (21)$$

The above optimization is summarized as Fig. 3. When applying the IPSO algorithm, positions of the particles are represented by the spatial coordinates of the machining positions labeled as the displacements in x, y, and z directions. The fitness value is set as the axial critical cutting depth which can be calculated by Eq. (6). According to Fig. 2, the spindle speed is firstly taken as the global variable. At a certain spindle speed, the IPSO algorithm controls the particles' positions, and the Kriging model predicts the corresponding modal parameters to calculate the fitness value based on the milling stability theory. Thus, the machining position with a higher axial critical

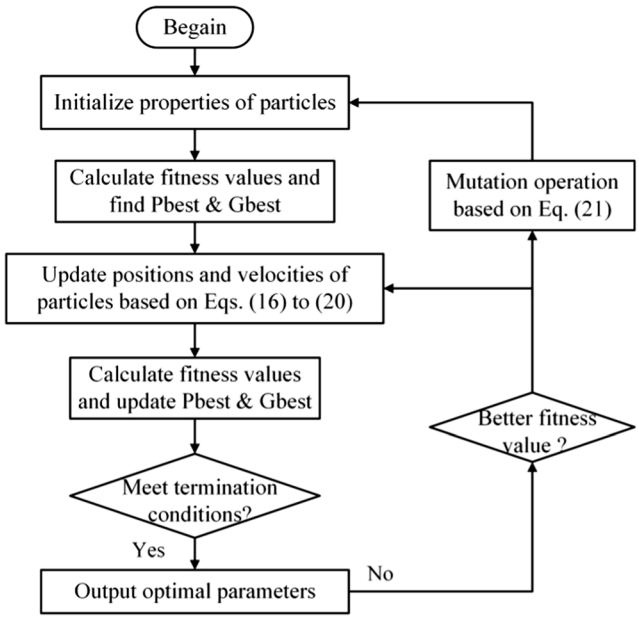

Fig. 3 Flow chart of the IPSO algorithm

cutting depth is searched in whole machine tool work volume. Then, the optimization moves to another spindle speed.

3 Robust milling chatter stability

Milling operation is a dynamic process, in which several parameters such as tool tip FRFs and cutting force coefficients are not constant. Considering the effects of varying parameters, a robust prediction of milling chatter stability is developed by extending the traditional chatter stability theory, based on the Edge theorem and the Zero Exclusion principle. The Edge theorem can be utilized to predict the uncertain time-delay systems that contain parameters varying within a certain range bounded by a minimum and maximum extreme value. According to the Edge theorem, for a polynomial with uncertain parameters, p, every combination of the extreme values will form a family of polynomials. These extreme polynomials are evaluated at a given frequency to form the vertices in the complex plane. If the edges between each pair of vertices are stable, then the system is robustly stable.

For applying the Edge theorem to the prediction of milling stability, Eq. (4) is transformed into the following form by ignoring the effects of cross FRFs:

$$a_0\Lambda^2 + a_1\Lambda + 1 = 0 \tag{22}$$

where

$$\begin{aligned} a_0 &= G_{xx}G_{yy}\left(a_{xx}a_{yy} - a_{xy}a_{yx}\right) \\ a_1 &= a_{xx}G_{xx} + a_{yy}G_{yy} \end{aligned} \tag{23}$$

Equation (22) represents the characteristic equation, and can be expanded in the Laplace domain to obtain Eq. (24) by introducing Eq. (7). The denominator of the transfer function with the dominant mode in Eq. (7) is multiplied on both sides of Eq. (24) to have a polynomial form, which is the system polynomial and expressed as Eq. (25). Then, every combination of the extreme values of the uncertain parameters is substituted to Eq. (25) to get the family of polynomial equations, P. In this research, modal parameters of the dominant modes in x and y directions and the cutting force coefficients in radial and tangential directions are assumed to vary within their minimum and maximum values. Thus, different combinations of the extreme values will form the family of polynomials as Eq. (26):

$$\begin{aligned} 0 = {} & G_{xx}(s,\omega_n)G_{yy}(s,\omega_n)\left(\alpha_{xx}\alpha_{yy} - \alpha_{xy}\alpha_{yx}\right)\left(-\frac{N}{4\pi}aK_{tc}\left(1-e^{-sT}\right)\right)^2 \\ & + \left(\alpha_{xx}G_{xx}(s,\omega_n) + \alpha_{yy}G_{yy}(s,\omega_n)\right)\left(-\frac{N}{4\pi}aK_{tc}\left(1-e^{-sT}\right)\right) + 1 \end{aligned} \tag{24}$$

$$\begin{aligned} 0 = {} & \left[G_{xx}(s,\omega_n)G_{yy}(s,\omega_n)\left(\alpha_{xx}\alpha_{yy} - \alpha_{xy}\alpha_{yx}\right)\left(-\frac{N}{4\pi}aK_{tc}\left(1-e^{-sT}\right)\right)^2 + \left(\alpha_{xx}G_{xx}(s,\omega_n) + \alpha_{yy}G_{yy}(s,\omega_n)\right)\left(-\frac{N}{4\pi}aK_{tc}\left(1-e^{-sT}\right)\right) + 1\right] \\ & \times\left(s^2 + 2\xi_i\omega_{n,i}s + \omega_{n,i}^2\right) \end{aligned} \tag{25}$$

$$\begin{aligned} P &= \left\{p_1(s,v), p_2\left(s,v\right), \cdots, p_i\left(s,v\right)\right\} \\ v &= [\omega_n, \xi, k, K_{tc}, K_{rc}] \Leftarrow \begin{cases} \omega_n \in [\omega_{n\min}, \ \omega_{n\max}] \\ \xi \in [\xi_{\min}, \ \xi_{\max}] \\ k \in [k_{\min}, \ k_{\max}] \\ K_{tc} \in [K_{tc\min}, \ K_{tc\max}] \\ K_{rc} \in [K_{rc\min}, \ K_{rc\max}] \end{cases} \end{aligned} \tag{26}$$

where i is the number of equations. If the number of uncertainties is k, i equals 2^k.

With Eq. (26), vertices can be calculated at each given frequency. The Zero Exclusion principle states a graphical technique to evaluate the stability of the edges efficiently. It states that if the zero of the complex plane is not located within the polygon generated by forming edges between each vertex, the system is stable. A four-sided polygon shown in Fig. 4 is taken as an instance. In order to check whether the zero lies in the interior of the polygon, a method based on quadrant distributions and

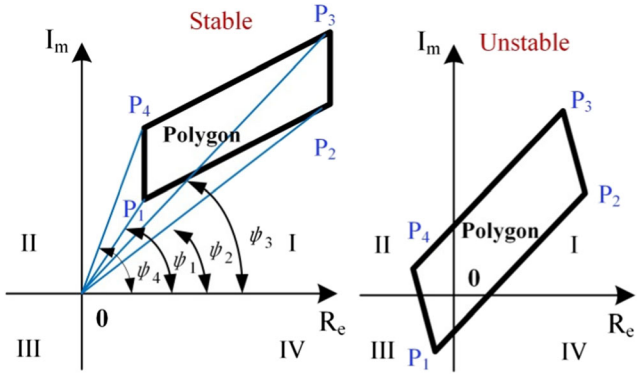

Fig. 4 Relationships between origin and polygon

arguments of the vertices is proposed. Five cases are studied as follows:

- Case I: All vertices locate in the same quadrant, and the system is stable as the zero is outside the polygon.
- Case II: Vertices locate in two adjacent quadrants as I-II, II-III, III-IV, and IV-I, and the system is stable.
- Case III: Vertices locate in diagonal quadrants as I-III and II-IV.
- Case IV: Vertices locate in three quadrants as I-II-III, II-III-IV, III-IV-I, and IV-I-II.
- Case V: Vertices locate in four quadrants, and the system is unstable as the zero is enclosed.

The minimum and maximum argument of each quadrant labels as φ_k^- and φ_k^+ respectively ($k = 1, 2, 3,$ and 4). For case III, k equals 1 or 2, and the system is stable if $\varphi_{k+2}^+ - \varphi_k^- < \pi$ or $\varphi_{k+2}^- - \varphi_k^+ > \pi$. For case IV, the conditions for obtaining the stable system are expressed in Table 1.

Therefore, the robust milling stability prediction is transformed into a graphical problem. Uncertainties are deliberately introduced into the nominal modal parameters and cutting force coefficients. At each spindle speed, the nominal values of the modal parameters are derived from the tool tip FRFs at the related optimal position. An algorithm summarized in Fig. 5 is developed to obtain the chatter stability lobe boundary based on the above formulations of the robust prediction. For a given cutting depth and spindle speed, a frequency range is determined, and the extreme polygon at each frequency is calculated and graphically checked. If the formed polygon is stable for all frequencies, the cutting depth is increased, and the aforementioned procedure is repeated until an unstable point is detected. The related cutting depth is recorded as the limit for the current spindle speed. Then, the algorithm moves onto the next spindle speed to detect another unstable point. For each combination of spindle speed, cutting depth, and frequency, the system stability is detected through the algorithm, until the focused spindle speed range is swept.

4 Case study and discussion of results

The above-described techniques for better prediction of robust chatter stability are applied to a real three-axis vertical machining center. In the case studies, first, machine tool FE model is constructed and analyzed to obtain sample information. Second, the Kriging model and IPSO algorithm are combined to predict the optimal machining positions in the spindle speed range. Finally, the upper and lower bounds of the uncertainties are determined, and then the robust chatter stability is predicted and discussed.

Table 1 Conditions for a stable system

Quadrant	Condition
I-II-III	$\varphi_3^+ - \varphi_1^- < \pi$
II-III-IV	$\varphi_4^+ - \varphi_2^- < \pi$
III-IV-I	$\varphi_3^- - \varphi_1^+ < \pi$
IV-I-II	$\varphi_4^- - \varphi_2^+ < \pi$

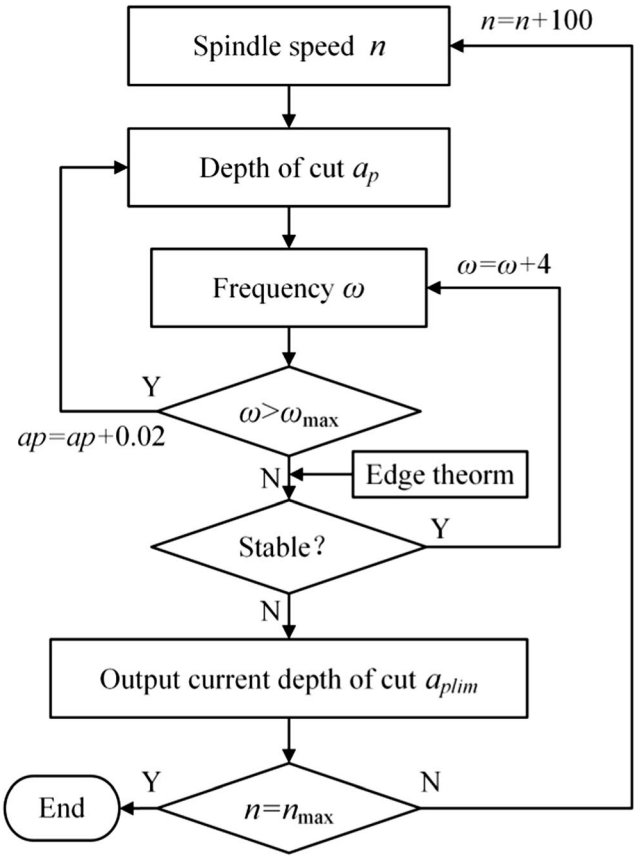

Fig. 5 Flow chart of the algorithm for robust chatter prediction

4.1 FE analysis within machine tool work volume

For the studied machining center, the movements of worktable, saddle, and headstock in x, y, and z directions respectively contribute to the varying machining position. The related travel limitations are x-0.4, y-0.55, and z-0.4 mm. The spindle speed range is from 0 to 15,000 rpm. Since it is experimentally difficult to directly identify the operational tool tip responses, FE technique is used to simulate the operational state. As the machine tool is an assembly, the joints dynamics at the connecting interfaces are first identified to establish an accurate FE model. These joints include linear guide joints, bolt joints, bearing joints, and ball screw joints, and their dynamic properties are simulated by spring-damper elements as shown in Fig. 6.

These joints connect conditions and approaches to identify these dynamic parameters were concretely discussed earlier by the authors in refs. [33–35]. The identified dynamic

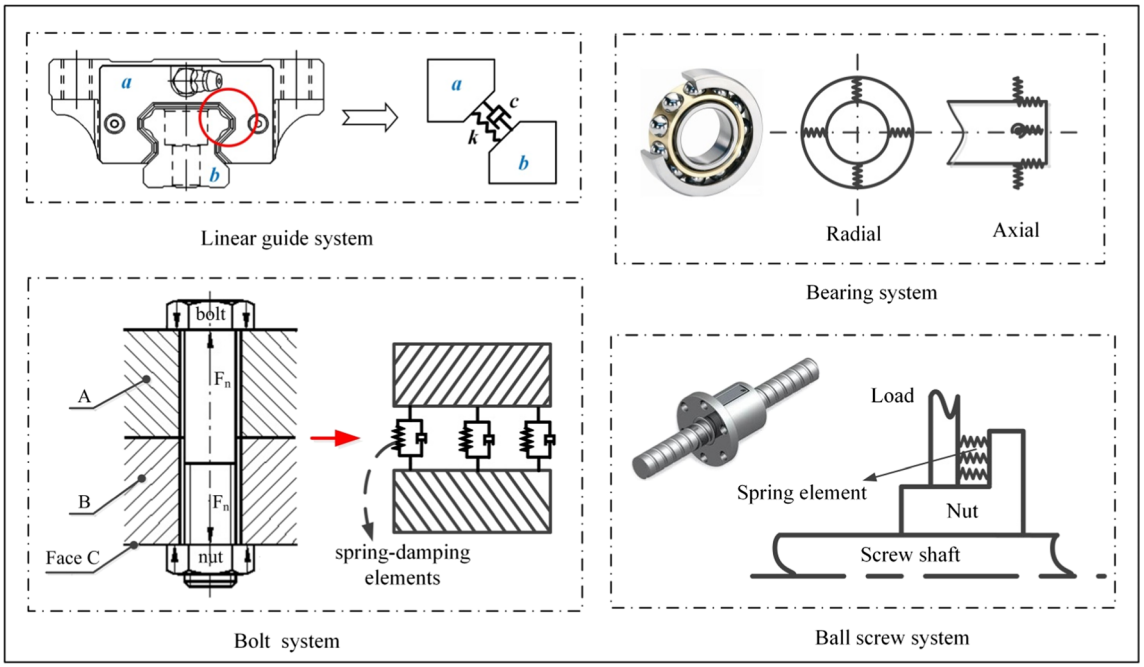

Fig. 6 Joints in machine tool and their equivalent forms

stiffness and damping coefficients for the linear guide joints are 6.07×10^8 N/m and 5280 N•s/m respectively. The axial stiffness between the nut and screw obtained from the manufacturer is 7.33×10^8 N/m. The bolt joints dynamic properties are identified based on the measured FRFs using the substructuring method; the obtained normal and tangential stiffness coefficients for the key bed-column joint are 4.9×10^{10} N/m and 6.9×10^9 N/m, respectively, and the obtained normal and tangential damping coefficients are 1.1×10^6 N•s/m and 9.8×10^4 N•s/m, respectively; and these bolt joints dynamic parameters are applied to the machine tool FE model to obtain the natural frequencies and the spindle tip FRFs, and small differentials between the simulated and tested results were observed [36].

The dynamic model of the spindle-holder-tool assembly is described in Fig. 7, and the identified dynamic interface parameters for the idle state are given in Table 2 [25, 37]. For the spindle bearing joints, the front and rear bearings are the same type and their basic information are described in Table 3. Since the centrifugal forces and gyroscopic moments caused by high spindle speeds will change the bearing dynamics [38–40], the algorithm proposed in [41] is used to calculate the axial and radial bearing translational stiffness described in Fig. 8. An inflection point is observed for the radial stiffness curve, and this phenomenon can be ascribed to the following reason: when the heat effect is ignored, the centrifugal force of the roller increases as the spindle speed increases, and then the inner ring and outer ring contact angle increases and decreases respectively as shown in Fig. 9; under this condition, the contact load between the roller and the inner ring decreases while the contact load between the roller and outer ring increases, but the radial stiffness still has a decrease; however, as the spindle speed further increases, the centrifugal force increases sharply and the roller begins to climb along the inner ring (the direction of the movement shown in Fig. 9); thus, the inner ring contact load and the radial stiffness increase instead; therefore, in a wide spindle speed range, the radial stiffness will initially decrease and then begin to increase above a critical speed value. In addition, the calculated speed-dependent radial stiffness curves under different preloads show that a higher preload corresponds to an inflection point with a higher spindle speed. Since the studied bearing preload is 96 N (an extra light preload), the inflect point of the radial stiffness occurs at a lower spindle speed (around 10,000 rpm).

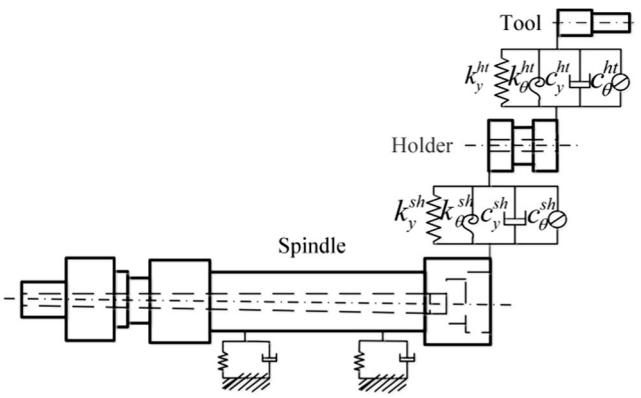

Fig. 7 Dynamic model of the spindle-holder-tool assembly

Taking the three-dimensional displacements and the spindle speed as the variables, 27 positions with the coordinates in Table 4 are arranged, and six spindle speed values at each position are determined [25]. The spindle speed samples are

Table 2 Dynamic properties of the spindle-tool-holder interfaces

	Translational stiffness (N/m)	Rotational stiffness (N• m/rad)	Translational damping (N• s/m)	Rotational damping (N•m• s/rad)
Spindle-holder interface	5.79×10^8	4.21×10^6	76	142
Tool-holder interface	6.25×10^7	3.86×10^6	175	0.14

Table 3 Basic parameters of the bearings

Type	Outer diameter D/mm	Inner diameter *d*/mm	Width *B*/mm	Contact angle β	Combination type	Preload *P*/N	Stiffness of bearing	
							Axial/(N/m)	Radial(/N/m)
7012C	95	60	18	15	2 row (DB)	96	0.53×10^8	3.45×10^8

0, 3000, 6000, 9000, 12,000, and 15,000 rpm respectively. The radial and axial stiffness related to these spindle speeds are given in Table 5. The machine tool FE model shown in Fig. 10 was reconstructed to meet the machining positions. At each position, the bearing stiffness related to the spindle speed samples were applied to the FE model in sequence to perform the modal and harmonic response analyses. Therefore, each FE model considered the spindle speed effects on bearing stiffness, and the related tool tip responses were obtained in both *x* and *y* directions. The direct tool tip FRFs vary with different operational conditions. For instance, Fig. 11a provides the FRFs at the column's top, middle, and bottom positions in *x* and *y* directions under stationary conditions, and Fig. 11b describes the FRFs related to three different spindle speeds at the same position. Shifts in natural frequencies and variations in amplitudes are observed. Investigating all the obtained FRFs at the 27 positions in the focused frequency range, four modes were determined for each direction. The identified natural frequencies, modal stiffness, and damping ratios in *x* and *y* directions were taken as the 162×24 sample responses matrix *Y*, and the related coordinates and spindle speed values were taken as the 162×4 sample inputs matrix *T*.

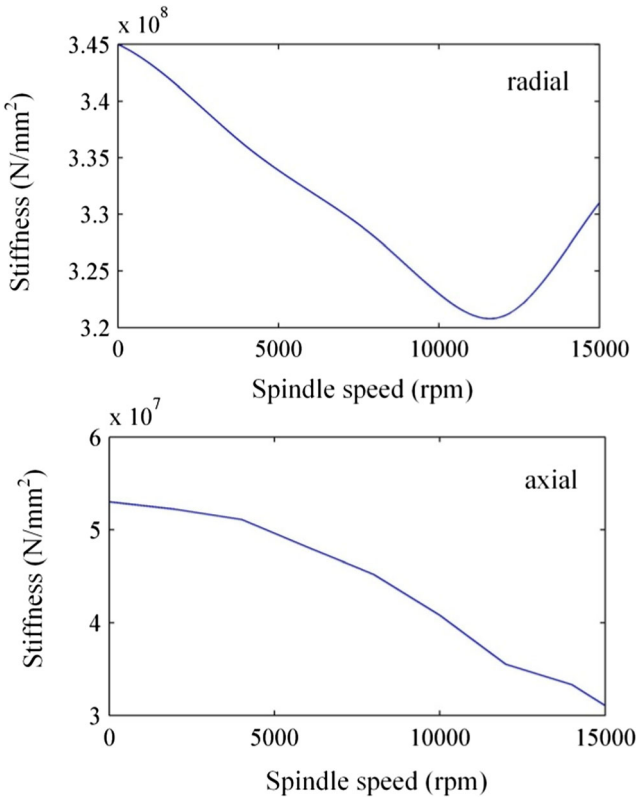

Fig. 8 Calculated operational bearing stiffness

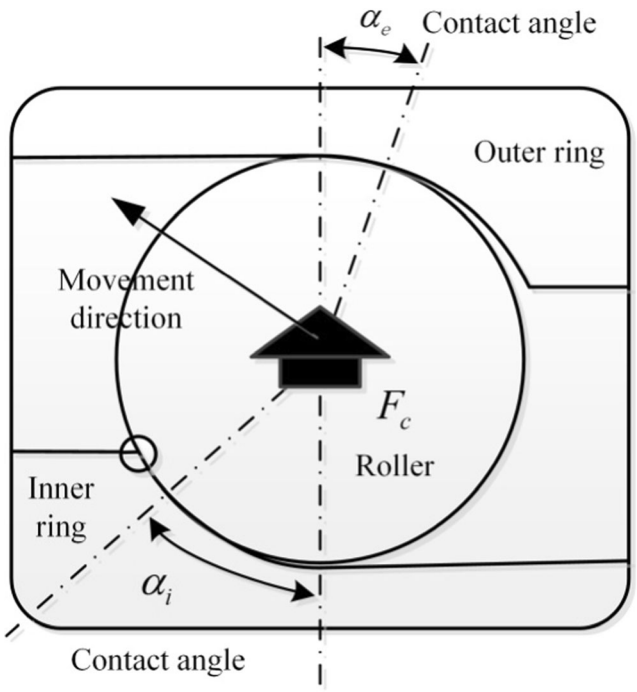

Fig. 9 Geometry of an angular contact ball bearing under operational state

Table 4 Experiment plan and the sample information

No.	Displacement/mm			No.	Displacement/mm			No	Displacement/mm			No	Displacement/mm			No	Displacement/mm		
	x	*y*	*z*		*x*	*y*	*z*		*x*	*y*	*z*		*x*	*y*	*z*		*x*	*y*	*z*
1	380	530	380	7	20	530	380	13	200	530	200	19	380	530	20	25	20	530	20
2	380	275	380	8	20	275	380	14	200	275	200	20	380	275	20	26	20	275	20
3	380	20	380	9	20	20	380	15	200	20	200	21	380	20	20	27	20	20	20
4	200	20	380	10	20	20	200	16	380	20	200	22	200	20	20				
5	200	275	380	11	20	275	200	17	380	275	200	23	200	275	20				
6	200	530	380	12	20	530	200	18	380	530	200	24	200	530	20				

4.2 Optimal combination of machining position and spindle speed

Based on previously determined matrix *Y* and *T*, a two-order polynomial was adopted to determine the regression model, and the widely used Gauss function was first utilized to calculate the correlations. The correlation function parameters θ_x, θ_y, θ_z, and θ_n were solved with MATLAB toolbox, and they were 3.46, 0.56, 8.23, and 10.68 respectively. Then, a Kriging predictor was established to calculate the modal parameters dependent on the machining position and spindle speed. For validation purposes, six positions labeled as *a*, *b*, *c*, *d*, *e*, and *f* in Fig. 10 were selected to perform the impact testing with an impact hammer (PCB 086D05, sensitivity of 0.23 mV/N). The vibration of a relatively rigid carbide end mill whose diameter was 25 mm with 80 mm gauge length and four teeth was measured at the tool tip using an accelerometer (ICP, sensitivity of 99.8 mv/g) with mass of 4.0 g. Since the tool diameter and gauge length were relatively larger, tool tip responses were measured under stationary conditions assuming that the mass of the accelerometer had a negligible effect on the dynamics [42]. The tested and predicted modal parameters in *x* direction are provided in Fig. 12. Smaller deviations indicate that the Kriging predictor has a reasonable accuracy.

To obtain the optimal combinations of machining position and spindle speed, the spindle speed was initially taken as the global variable ranging from 0 to 15,000 rpm, and it was discretized at an interval of 100 rpm according to Section 2.3. At each certain spindle speed, the IPSO algorithm controlled the variations of the machining position; then, the position and speed-dependent tool tip FRFs were reorganized based on the modal fitting technique and the modal parameters predicted by the validated Kriging model; the reorganized FRFs were applied into the analytical milling stability model to calculate the axial critical cutting depths, and these calculated values were compared after each iteration; the higher values were used to update the particle best and global best, and then the iteration moved on to another; when the number of iterations met the upper limit, the final global best was the optimal machining position. The entire optimization terminated until the spindle speed met its upper limit.

For the IPSO algorithm, the number of the particle swarm was initialized as 50, and each particle had three dimensions representing the displacements of *x*, *y*, and *z* directions. The initial value w_{max} and w_{min} were 0.9 and 0.4, c_1 and c_2 were both set as 2, and the number of iterations was 400. The displacement limits of three directions were used as the constraints. And the particles' initial positions and velocities were set randomly and further updated based on Eqs. (16) to (21). The updates depended on the fitness values calculated from the milling stability theory through Eqs. (1) to (6). The stability analysis was for end milling ASTM 1045 steel with the cutter of four teeth; the tool tip FRFs were reorganized from the modal parameters predicted by the established Kriging model; the radial immersion and feed values were set as constants for simplicity; and the tangential and radial cutting force coefficients of the work-material were 1977 and 754 MPa respectively.

The obtained stability lobe diagram describing relationships between the spindle speed and the cutting depth is shown in Fig. 13. This SLD is compared with another SLD, which is plotted at the column's middle position under stationary condition using the conventional analytical chatter

Table 5 The speed-dependent bearing stiffness for the samples

Bearing stiffness ($\times 10^8$ N/m)	Spindle speed (rpm)					
	0	3000	6000	9000	12,000	15,000
Radial	3.45	3.39	3.32	3.26	3.21	3.30
Axial	0.53	0.51	0.48	0.43	0.36	0.31

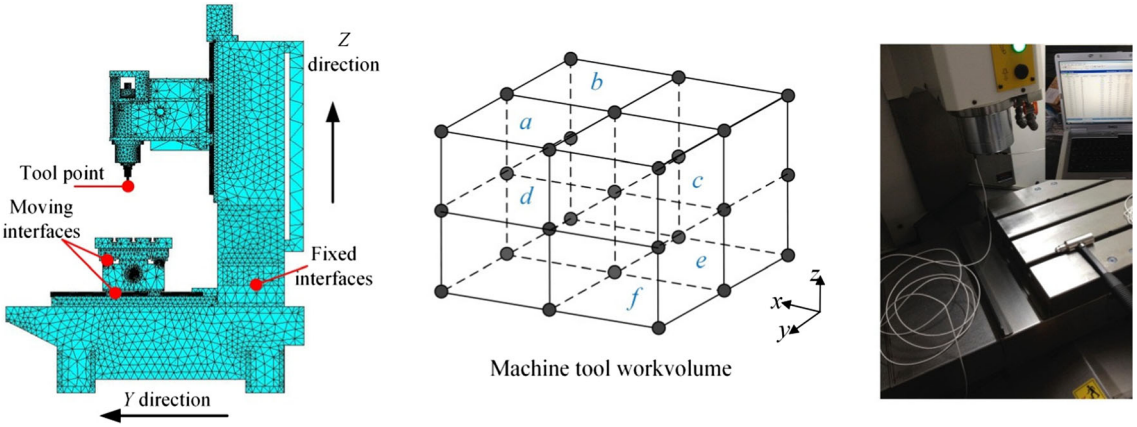

Fig. 10 Whole machine tool and its FEM

stability theory. As seen from Fig. 13, distinct deviations occurred as the machining position and spindle speed varied.

4.3 Robust chatter prediction at optimal position

In the milling process, modal parameters and cutting force coefficients are uncertainties. According to the Edge theory, the number of polynomials is determined by the number of uncertainties. As the tool tip FRFs usually have more than one mode, taking all modal parameters into consideration will increase the number of polynomials and add practical difficulties to the robust chatter prediction. Therefore, for simplicity, dynamic parameters for one mode are assumed to simultaneously reach their maximum and minimum values. Since the studied tool tip FRFs has four modes, the natural frequencies, damping ratios, and modal stiffness in x and y directions determine eight sets of uncertainties. The tangential and radial cutting force coefficients determine two uncertainties. An automated algorithm aforementioned in Section 3 was developed in MATLAB software to predict and plot the robust chatter stability lobe, which was composed by the predictions at each combination of machining position and spindle speed. For each combination, the initial cutting depth was 0, and an increment of 0.01 mm was set. The frequency range was from 200 to 2000 Hz, and an increment of 10 Hz was set. The algorithm terminated until the spindle speed met the upper limit.

When determining the upper and lower bounds of the modal parameters, effects of the machining allowances are considered since the tool will move deviating from the optimal machining position. At each spindle speed, taking the related optimal position as a standard value, the limiting displacements of the tool motions in three directions may form a small

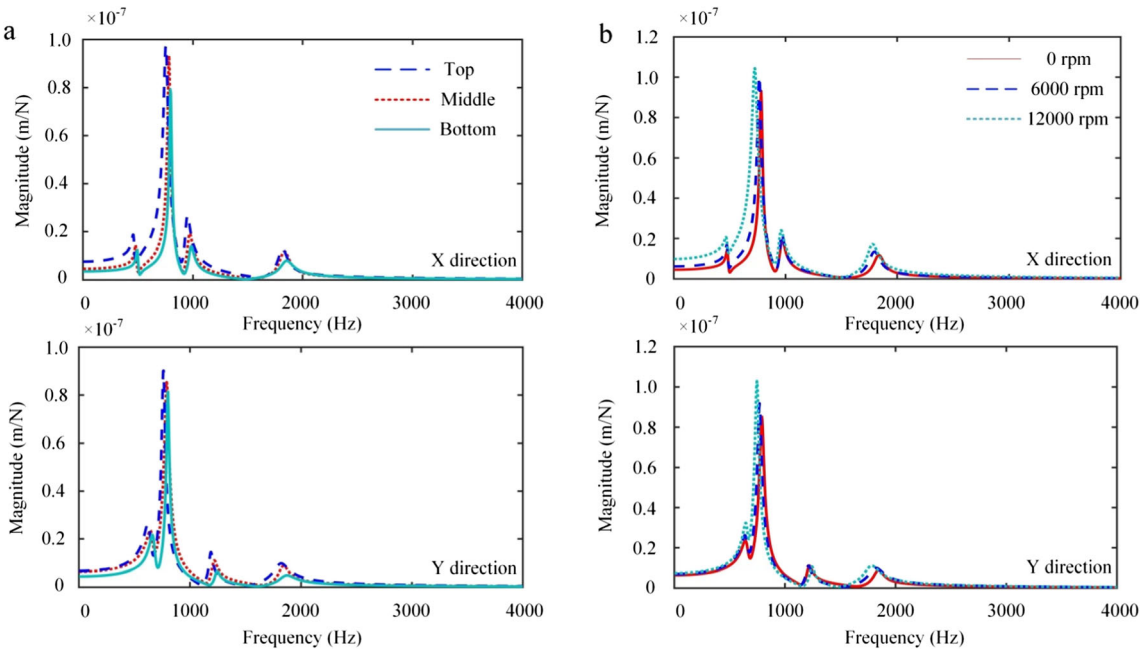

Fig. 11 **a** Comparisons of FRFs at top, middle, and bottom positions. **b** Comparisons of FRFs at different spindle speed values

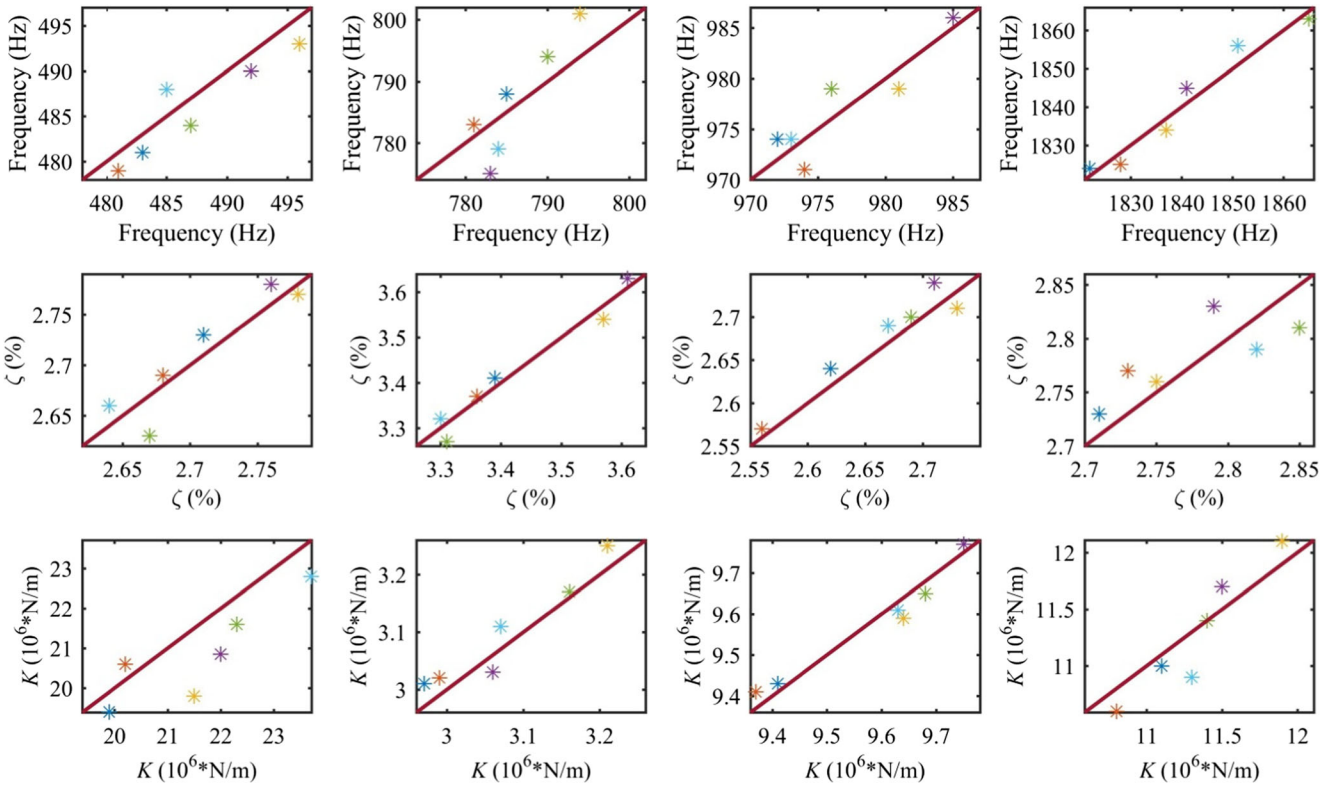

Fig. 12 Validation of the Kriging model

machining box as shown in Fig. 14, in which the maximum and minimum values of the position and speed-dependent modal parameters are searched based on the Kriging model. These extreme values are regarded as the initial left and right worst-case deviations of uncertain modal parameters. Further considering that other factors will introduce uncertainties, such as the simulation errors and thermal effects, another ± 3% variation for each parameter was taken for simplicity. For instance, at a given optimal position, the three-dimensional information of the machining box is $180 \times 120 \times 50$ mm^3, and the identified extreme values are listed in Table 6. The ultimate upper and lower bounds of the modal parameters are also summarized in Table 6. For the cutting force coefficients 1977 and 754 MPa, they were identified based on the tested average cutting forces and the analytic force model. The constant coefficients are not applicable for different combinations of the machining parameters. Thus, a ± 5% variation was taken for the tangential and radial cutting forces coefficients considering the effects due to theoretical error, tool wear, measurement technology, and so on. Therefore, with the founded

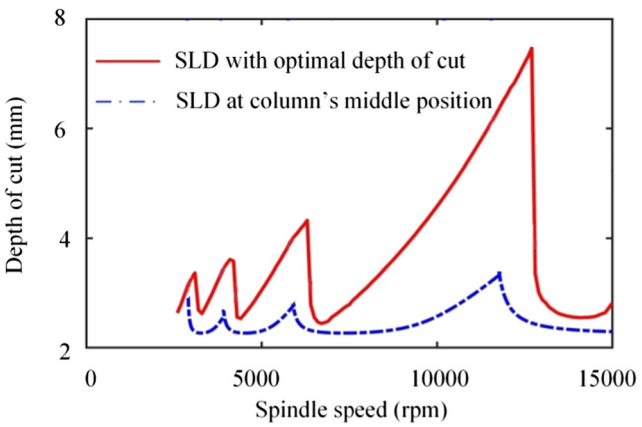

Fig. 13 Comparisons of different stability lobes

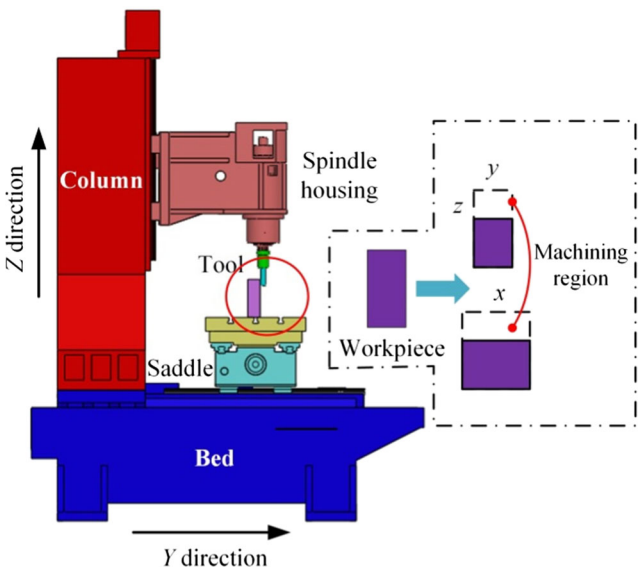

Fig. 14 Description of machining box

Table 6 Modal parameters and their limits at a given optimal position

Direction	Modes	Natural frequency, f (Hz)		Damping ratio, ξ (%)		Modal stiffness, K ($\times 10^6$ N/m)	
X	1	484	↑ 492 × (1 + 3%)	2.72	↑ 2.77 × (1 + 3%)	20.3	↑ 20.8 × (1 + 3%)
			↓ 474 × (1–3%)		↓ 2.64 × (1–3%)		↓ 19.5 × (1–3%)
	2	784	↑ 801 × (1 + 3%)	3.57	↑ 3.64 × (1 + 3%)	3.34	↑ 3.42 × (1 + 3%)
			↓ 758 × (1–3%)		↓ 3.51 × (1–3%)		↓ 3.27 × (1–3%)
	3	968	↑ 985 × (1 + 3%)	2.62	↓ 2.68 × (1 + 3%)	9.58	↑ 9.76 × (1 + 3%)
			↓ 957 × (1–3%)		↑ 2.56 × (1–3%)		↓ 9.43 × (1–3%)
	4	1836	↑ 1877 × (1 + 3%)	2.65	↑ 2.71 × (1 + 3%)	11.2	↑ 11.6 × (1 + 3%)
			↓ 1793 × (1–3%)		↓ 2.59 × (1–3%)		↓ 10.7 × (1–3%)
Y	1	656	↑ 671 × (1 + 3%)	3.51	↑ 3.57 × (1 + 3%)	8.84	↑ 9.07 × (1 + 3%)
			↓ 644 × (1–3%)		↓ 3.45 × (1–3%)		↓ 8.65 × (1–3%)
	2	792	↑ 818 × (1 + 3%)	2.41	↑ 2.47 × (1 + 3%)	2.04	↑ 2.10 × (1 + 3%)
			↓ 775 × (1–3%)		↓ 2.34 × (1–3%)		↓ 2.03 × (1–3%)
	3	1216	↑ 1241 × (1 + 3%)	1.69	↑ 1.76 × (1 + 3%)	29.5	↑ 30.2 × (1 + 3%)
			↓ 1190 × (1–3%)		↓ 1.63 × (1–3%)		↓ 28.5 × (1–3%)
	4	1844	↑ 1882 × (1 + 3%)	3.80	↑ 3.91 × (1 + 3%)	12.3	↑ 12.6 × (1 + 3%)
			↓ 1796 × (1–3%)		↓ 3.69 × (1–3%)		↓ 11.7 × (1–3%)

system parameters and their variations, the robust chatter stability lobe diagram was plotted and outlined in Fig. 15.

4.4 Experiments and discussion

Using the real milling system in Fig. 8, chatter tests were performed with different combinations of spindle speed and cutting depth to detect if chatter occurred. During machining, a microphone and a dynamometer were used to measure the sound and force signals. Based on the sensor data acquired in the frequency domain, the occurrence of chatter was determined for each spindle speed and cutting depth combination. For stable condition, changes in these signals are less prominent with a noticeable variation in magnitude and peaks occur less often. And the tooth passing frequency shown in Fig. 16b can be observed. Therefore, when chatter is detected, a prominent peak occurs at a chatter frequency can be observed. For instance, the spectrogram for the combination of spindle speed 10,000 rpm and cutting depth 4.05 mm is described in Fig. 16a, where a sudden peak occurs around 756 Hz near the dominant vibrational mode of the tool tip; besides, in the force spectrum described as Fig. 16c, a peak around 738 Hz is also observed.

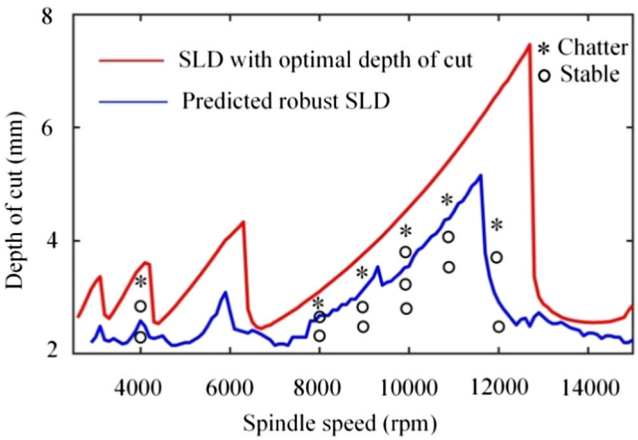

Fig. 15 Predicted robust chatter stability lobe

Determinations of whether chatter occurred were swept through the arranged machining combinations, and the results are labeled in Fig. 15. The figure shows that majority of the chatter-free points are below the robust boundary, indicating that the experimental chatter tests have a good correlation to the predicted robust stability lobe. To further illustrate the feasibility of the predicted robust SLD, the obtained SLD with the optimized depths of cut in Fig. 13 is also plotted in Fig. 15. It can be observed that many of the detected unstable points locate below the boundary of the optimal lobe. Since uncertain parameters may fall anywhere within a given range in real machining, stable and unstable points are both observed in the region between these two SLDs. This shows the main advantage of the proposed robust chatter evaluation method in that it predicts the milling stability more conservatively. The robust prediction considers the effects caused by variations of uncertain parameters in the full range, and then produce the relatively conservative combinations of spindle speeds and depths of cut to ensure a stable machining with higher operational reliability. However, since the robust prediction is based on the optimal combinations of machining positions and spindle speeds, it still has a higher stability limit when compared with the conventional SLD such as the one plotted in Fig. 13. Accordingly, using the robust SLD to guide the selections of cutting parameters will enhance the practicality, for the conventional stability lobes are only applicable for milling system with a constant value of parameters.

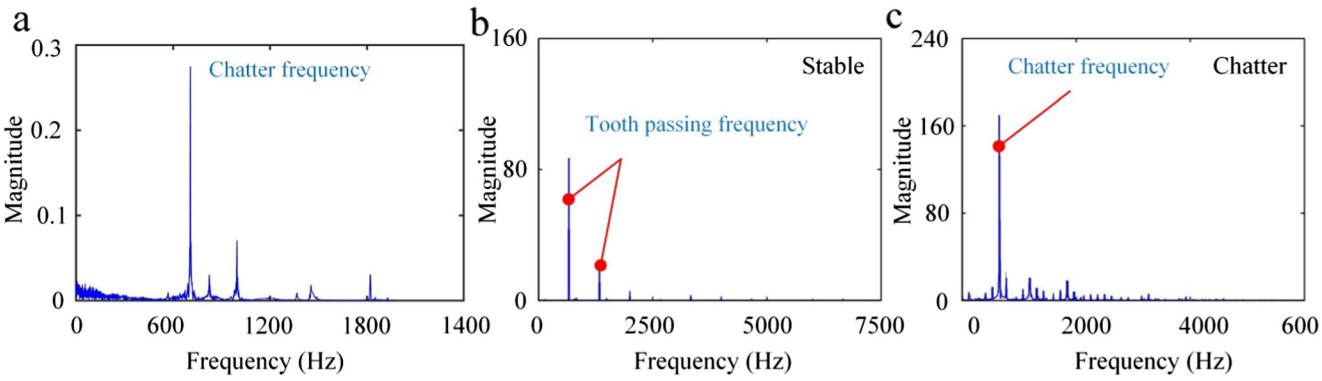

Fig. 16 **a** Sound spectrum under chatter condition. **b** Force spectrum for the stable condition. **c** Sound spectrum under chatter condition

5 Conclusion

Regenerative chatter is a common vibration phenomena occurred in real machining, which can affect the machining quality, limit the productivity, and damage the cutting system. Accordingly, accurate chatter prediction is significant in milling operations. Under operational state, the system dynamics and cutting force coefficients may become uncertain parameters. Variations in these system parameters severely affect the prediction accuracy, since the conventional mathematical model describing chatter vibrations are based on the assumption that the system parameters are constant. This paper demonstrates an analytical method for robust prediction of the chatter stability lobe, in which the optimal configurations of the machining positions and the spindle speeds are taken into account. Therefore, the FE technique is initially combined with the modal fitting technique to establish a Kriging model to reorganize the tool tip FRFs dependent on machining position and spindle speed; the IPSO algorithm is used to search the position with the highest cutting depth at each given spindle speed using the traditional milling stability theory; and then, the robust chatter prediction is performed at these optimal positions by extending the milling stability theory based on the Edge theorem and the Zero Exclusion principle. For this research, uncertainties are artificially introduced into the modal parameters of tool tip FRFs and the cutting force coefficients. Based on every combination of extreme values of uncertain parameters, a robust chatter stability lobe with relatively higher cutting depths is simulated ultimately.

Chatter tests were carried out on a three-axis vertical machining center to validate the proposed method. Different combinations of the spindle speed and cutting depth were determined from the obtained robust SLD to perform the chatter tests. Occurrences of the chatter were detected by studying the frequency spectrums of the sound and force information. The experimental results show that all combinations below the lobe boundary and partial combinations above the lobe boundary can provide a stable machining. This indicates that the robust prediction may not capture all stable points; however, it allows a conservative chatter stability prediction to ensure the reliability. These experimental results were also compared to the optimized conventional stability lobe. Unstable points were still observed below the boundary of the conventional SLD, further validating that the robust prediction can simulate a boundary below which the stability is guaranteed. The proposed robust chatter prediction method may be easier to apply and provide more reliable results. Nevertheless, the boundary of the stability lobe is still dependent upon the accuracy of the uncertainty bounds on system parameters, which are difficult to be determined in practice. Additionally, since only the tool tip FRFs are considered in the robust chatter prediction, the proposed method is not appropriate for the machining condition that the workpiece system is less rigid than the tool system. Accordingly, in further research, taking the dynamic properties of the workpiece system into consideration and conducting an investigation into obtaining more accurate extreme values of the uncertainties and extending the robust approach to consider more changing parameters are the main subjects.

Funding information This research is supported by the National Natural Science Foundation of China under Grant no. 51705058, the Science and Technology Research Program of Chongqing Municipal Education Commission under Grant no. KJ1704087, and the Chongqing Research Program of Basic Research and Frontier Technology under Grant no. cstc2017jcyjAX0005.

References

1. Tlusty J, Polacek M (1963) The stability of machine tools against self-excited vibrations in machining. Proc ASME Int Res Prod Eng 1:465–474
2. Grossi N, Scippa A, Sallese L, Sato R, Campatelli G (2015) Spindle speed ramp-up test: a novel experimental approach for chatter stability detection. Int J Mach Tools Manuf 89(3): 221–230

3. Cao HR, Yue Y, Chen XF, Zhang XW (2017) Chatter detection based on synchrosqueezing transform and statistical indicators in milling process. Int J Adv Manuf Technol 1:1–12
4. Quintana G, Ciurana J (2011) Chatter in machining processes: a review. Int J Mach Tool Manu 51(5):363–376
5. Özşahin O, Budak E, Özgüven HN (2014) In-process tool point FRF identification under operational conditions using inverse stability solution. Int J Mach Tool Manu 89:64–73
6. Zhang XM, Ding H (2013) Note on a novel method for machining parameters optimization in a chatter-free milling process. Int J Mach Tools Manuf 72:11–15
7. Tobias SA, Fishwick W (1958) The chatter of lathe tools under orthogonal cutting conditions. Trans ASME 80(1):1079–1088
8. Altintas Y, Budak E (1995) Analytical prediction of stability lobes in milling. CIRP Ann Manuf Technol 44:357–362
9. Ding Y, Zhu LM, Zhang XJ, Ding H (2010) A full-discretization method for prediction of milling stability. Int J Mach Tools Manuf 50:502–509
10. Minis I, Yanushevsky R (1993) A new theoretical approach for the prediction of machine tool chatter in milling. J Eng Ind 115(1):1–8
11. Insperger T (2010) Semi-discretization method for delayed systems. Int J Numer Methods Eng 55(5):503–518
12. Altintas Y, Stepan G, Merdol D, Dombovari Z (2008) Chatter stability of milling in frequency and discrete time domain. CIRP J Manuf Sci Technol 1(1):35–44
13. Altintas Y, Weck M (2004) Chatter stability of metal cutting and grinding. CIRP Ann Manuf Technol 53(2):619–642
14. Sun Y, Sun J, Li J, Li W, Feng B (2013) Modeling of cutting force under the tool flank wear effect in end milling Ti6Al4V with solid carbide tool. Int J Adv Manuf Technol 69(9–12):2545–2553
15. Liu Y, Wang ZY, Liu K, Zhang YM (2017) Chatter stability prediction in milling using time-varying uncertainties. Int J Adv Manuf Technol 89(9–12):2627–2636
16. Duncan GS, Kurdi M, Schmitz TL, Snyder JP (2016) Uncertainty propagation for selected analytical milling stability limit analyses. Trans NAMRI/SME 34:17–24
17. Zhang XM, Zhu LM, Zhang D, Ding H, Xiong YL (2012) Numerical robust optimization of spindle speed for milling process with uncertainties. Int J Mach Tool Manu 61(1):9–19
18. Sims ND, Manson G, Mann B (2010) Fuzzy stability analysis of regenerative chatter in milling. J Sound Vib 329(8):1025–1041
19. Hamann D, Walz NP, Fischer A, Hanss M, Eberhard P (2018) Fuzzy arithmetical stability analysis of uncertain machining systems. Mech Syst Signal Process 98:534–547
20. Park SS, Qin YM (2007) Robust regenerative chatter stability in machine tools. Int J Adv Manuf Technol 33(3–4):389–402
21. Graham E, Mehrpouya M, Park SS (2013) Robust prediction of chatter stability in milling based on the analytical chatter stability. J Manuf Process 15(4):508–517
22. Graham E, Mehrpouya M, Nagamune R, Park SS (2014) Robust prediction of chatter stability in micro milling comparing edge theorem and LMI. CIRP J Manuf Sci Technol 7(1):29–39
23. Liu XL, Gao HN, Yue CX, Li RY, Jiang N, Yang L (2018) Investigation of the milling stability based on modified variable cutting force coefficients. Int J Adv Manuf Technol 96(9–12): 2991–3002
24. Law M, Altintas Y, Phani AS (2013) Rapid evaluation and optimization of machine tools with position-dependent stability. Int J Mach Tools Manuf 68:81–90
25. Deng CY, Miao JG, Wei B, Feng Y, Zhao Y (2018) Evaluation of machine tools with position-dependent milling stability based on Kriging model. Int J Mach Tool Manu 124:33–42
26. Oliver MA, Webster R (1990) Kriging: a method of interpolation for geographical information systems. Int J Geogr Inf Syst 4(3): 313–332
27. Mason DC, O"Conaill M, Mckendrick I (2012) Variable resolution block kriging using a hierarchical spatial data structure. Int J Geogr Inf Syst 8(5):429–449
28. Denimal E, Nechak L, Sinou JJ, Nacivet S (2016) Kriging surrogate models for predicting the complex eigenvalues of mechanical systems subjected to friction-induced vibration. Shock Vib 4:1–22
29. Schmitz B, Smith K (2009) Machining Dynamics: frequency response for improved productivity. Springer, US
30. Yi P, Wei KT, Kong XJ, Zhu Z (2015) Cumulative PSO-Kriging model for slope reliability analysis. Probab Eng Mech 9:39–45
31. Yang N, Jing YY (2015) Recognition of functions extreme optimization based on the improved PSO algorithm. Comput Simul 32: 263–266
32. Wu HY, Zhu CC, Chang BG (1999) Adaptive genetic algorithm to improve group premature convergence. J Xi'an Jiaotong Univ 33(11):27–30
33. Deng CY, Liu Y, Zhao J, Wei B, Yin GF (2017) Analysis of the machine tool dynamic characteristics in manufacturing space based on the generalized dynamic response model. Int J Adv Manuf Technol 92(1–4):1411–1424
34. Deng CY, Yin GF, Fang H, Meng ZYX (2015) Dynamic characteristics optimization for a whole vertical machining center based on the configuration of joint stiffness. Int J Adv Manuf Technol 76(5–8):1225–1242
35. Tan F, Yin GF, Dong GH, Wang L, Tan WX (2015) Optimized identification of bolt joint's tangential dynamic stiffness based on the substructure synthesis method. J Sichuan Univ (Eng Sci Ed) S2: 171–177
36. Deng CY, Heng L, Yin Q, Lin LJ, Yin GF (2015) Application of bolt joints dynamic parameters identification in machine tools based on partially measured frequency response functions. J Vibroeng 17(3):1090–1104
37. Ertürk A, Özgüven HN, Budak E (2006) Analytical modeling of spindle–tool dynamics on machine tools using Timoshenko beam model and receptance coupling for the prediction of tool point FRF. Int J Mach Tool Manu 46(15):1901–1912
38. Cao HR, Li B, He Z (2012) Chatter stability of milling with speed-varying dynamics of spindles. Int J Mach Tools Manuf 52(1):50–58
39. Özşahin O, Budak E, Özgüven HN (2015) Identification of bearing dynamics under operational conditions for chatter stability prediction in high speed machining operations. Precis Eng 42:53–65
40. Hung JP, Lai YL, Luo TZ (2013) Analysis of the machining stability of a milling machine considering the effect of machine frame structure and spindle bearings: experimental and finite element approaches. Int J Adv Manuf Technol 68:2393–2405
41. Hu T, Yin GF, Sun MN (2014) Dynamic performance of a shaft-bearing system with centrifugal force and gyroscopic moment effects. J Vib Shock 33(8):100–108
42. Özşahin O, Özgüven HN, Budak E (2010) Analysis and compensation of mass loading effect of accelerometers on tool point FRF measurements for chatter stability predictions. Int J Mach Tool Manu 50(6):585–589